Vietnam Journal of Earth Sciences, 41(3), 201–215, Doi: 10.15625/0866-7187/41/3/13829

(VAST)

Vietnam Academy of Science and Technology

**Vietnam Journal of Earth Sciences**

http://www.vjs.ac.vn/index.php/jse

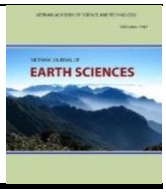


# Developing land-cover driver model for estimating the intensity of surface urban heat islands using landsat 8 satellite imagery

Nguyen Thanh Hoan, Nguyen Van Dung*, Ho Le Thu, Hoa Thuy Quynh

*Institute of Geography, VAST, Hanoi, Vietnam*

Received 1 October 2018; Received in revised form 11 April 2019; Accepted 18 May 2019

ABSTRACT

It is of utmost importance to understand and monitor the impact of urban heat islands on ecosystems and overall human health in the context of climate change and global warming. This research was conducted in a tropical city, Hanoi, with a major objective of assessing the quantitative relationships between the composition of the main land-cover types and surface urban heat island phenomenon. In this research, we analyzed the correlation between land-cover composition, percentage coverage of the land cover types, and land surface temperature for different moving window sizes or urban land management units. Landsat 8 OLI (Operational Land Imager) satellite data was utilized for preparing land-cover composition datasets in inner Hanoi by employing the unsupervised image clustering method. High-resolution (30 m) land surface temperature maps were generated for different days of the years 2016 and 2017 using Landsat 8 TIRS (Thermal Infrared Sensor) images. High correlations were observed between percentage coverage of the land-cover types and land surface temperature considering different window sizes. A new model for estimating the intensity of surface urban heat islands from Landsat 8 imagery is developed, through recursively analyzing the correlation between land-cover composition and land surface temperature at different moving window sizes. This land-cover composition-driven model could predict land surface temperature efficiently not only in the case of different window sizes but also on different days. The newly developed model in this research provides a wonderful opportunity for urban planners and designers to take measures for adjusting land surface temperature and the associated effects of surface urban heat islands by managing the land cover composition and percentage coverage of the individual land-cover types.

*Keywords:* Surface urban heat island; land cover; Landsat 8; regression; land management unit; tropics.



## 1. Introduction

In the context of climate change and global warming, it is of utmost importance to understand and monitor the impact of urban heat islands on ecosystems and overall human health. Urban heat island refers to the phenomenon of increased temperature in urban centers compared to their surrounding rural environments.

The phenomenon behind the urban heat island has been studied for a long time. This effect was described by Luke Howard in the 1810s (Howard 1833). From 1964 to 1968, Robert D. Bornstein used a helicopter to study

*Corresponding author, Email: nvdungvdl@gmail.com

the urban heat island of New York City and determined the effect of urban heat island in both vertical and horizontal directions. The results display maximum intensity of urban heat island near the ground surface and decrease to zero at a height of 300 m (Bornstein 1968). Ackerman (1985) studied the diurnal and seasonal variation in the Chicago urban heat island, recording an elevation averaging 1.85°C in temperature inside the city most of the time.

Due to easy access and wall-to-wall continuous coverage, LST derived from thermal infrared remote sensors is one of the most commonly used indicators for surface UHI (SUHI) analysis (Schwarz et al., 2012, Meng et al., 2018). In this study, the SUHI is defined as the magnitude of the temperature differentials between any two land-cover types, a more general way than that which is typically adopted in the literature. From the physical point of view, LST and air temperature are different entities, while strong correlations were found between them by many researchers in the literature (Schwarz et al., 2012; Galo et al., 2011). For a few decades, satellite data has been exploited for determining and explaining the heat island phenomenon observed in many cities around the world. Since the 1990s, 3D models have been made of the effects of surface urban heat island in Tokyo, Japan, using satellite and land survey data (Saitoh et al., 1996). In Nagoya, Japan, the seasonal changes pertaining to urban heat island have been analyzed using Landsat and ASTER images taken during the day as well as night, and these have been modeled to determine if the heat fluxes are natural or artificial (Kato and Yamaguchi, 2005). In Chicago, Landsat and MODIS images have been utilized in order to determine surface urban heat island. It was found that the temperature of the city center is warmer than the surrounding areas by nearly 5K. Higher negative correlation 0.64–0.71, the observed variance in different years between land surface temperatures (LST) and Normalized Difference Vegetation Index (NDVI) have also been reported (Mackey et al., 2012). In Washington, the temperature of the city center was found higher than the surrounding vegetative areas by up to 10°C (Kim 1992). These studies have indicated that vegetation cover plays a key role in minimizing the surface urban heat island effect.

In another study, the analysis performed with the help of Landsat data and field measurements has shown that the highest average surface temperature in Bangkok increased from 26.01°C in 1994 to 37.76°C in 2000 and further to 39.79°C in 2009 (Srivanit, Hokao and Phonekeo 2012). Many studies have also indicated a correlation between surface urban heat island and land-cover composition in a city. For example, Weng et al. (2004) reported a correlation between surface temperature and vegetation in Indianapolis, USA. Chen et al. (2006) examined the relationship between surface urban heat island and land-cover change, in certain cities of the Guangdong province in Southeast China, using Landsat images from 1990 to 2000. A similar study on the relationship between surface urban heat island, land-cover change, and population density was also conducted in Nagpur, India (Kotharkar and Surawar, 2015). Grover and Singh (2015) analyzed the relationship between NDVI and land surface temperature in Delhi and Mumbai, India, as well.

Other similar studies have also been conducted (Yuan and Bauer, 2007; Oke and Maxwell, 1975; Miao et al., 2009, Estoque et al., 2017; Singh et al., 2017). These studies have drawn similar conclusions that urban temperatures are highly correlated with land-

cover composition (water, vegetation, built-up, among others) in the cities.

Urban heat island is mainly caused by the modification of land surfaces and the concentration of population (Solecki et al., 2005; Zhou et al., 2018). The process of land modification generally increases the use of materials that retain heat (concrete surfaces) and sacrifices air-conditioning elements such as trees and water surface, and moreover, waste heat is generated by energy usage. In tropical cities, where there is a great number of very hot days, urban heat island has many negative effects on the quality of the living environment in these cities.

Urbanization and urban heat island have been a hot topic in Asia. In recent years, the effects of urban heat island have been noted in many cities. For example, the Hong Kong Observatory shows that the number of extremely hot days has increased noticeably in recent years, reaching a record of 38 very hot days in 2016 (www1). In India, hundreds of people died from heat strokes and hot temperatures up to 51°C in 2015 and 2016 (www2).

Hanoi, the capital of Vietnam, is one of the hottest cities in Asia, and it is highly susceptible to the detrimental consequences of heat island on urban ecology and human health. On June 4, 2017, Hanoi experienced a heat wave of the hottest level in the past 40 years, reaching 42°C (www3). According to the study, which characterized rainfall and temperature variability for all of Vietnam over 40 years from 1971 to 2010, Vietnam's average temperature has increased at a rate of $0.26 \pm 0.10$°C per decade since the 1970s, which is approximately twice the rate of global warming over the same period (Nguyen et al., 2014). In Vietnam, urban heat island has also been interested in by some scientists, which are concentrated in the two big cities, Hanoi and Ho Chi Minh City, such as Mai and Tang-Huang 2018, Nhung et al., 2017; Van and Xuan Bao, 2010; Van 2014; Van et al., 2017. However, there is still a lack of quantitative studies on the relationship between SUHI and land cover types.

This research has been conducted in a tropical city, Hanoi, with a major objective of assessing the quantitative relationships between the composition of the main land-cover types and surface urban heat island phenomenon. This research analyzes the effects of land-cover composition on surface urban heat island on extremely hot days and discusses the measures applicable for minimizing the urban temperature conditions.

## 2. Methodology

### *2.1. Study area*

This research was conducted in inner Hanoi, which is the capital city of Vietnam, encompassing an area of 160 km$^2$. The location of the study area is illustrated in Fig. 1.

The selected study area covers most of the high-density built-up areas of Hanoi. In addition, water surface and agricultural cropland areas were also selected large enough to have sufficient data for comparing land surface temperatures between different land cover types.

Hanoi is inhabited by more than 7 million people and has a high population density (11,220 people/km$^2$) in urban districts. Hanoi is located in a tropical belt; thus, summers are very hot with an average temperature of 32°C lasting from May to August, and July is the hottest month. The average number of very hot days (> 35°C) from 1961 to 2007 was 21days, and that has increased in recent years (Huong et al., 2010).

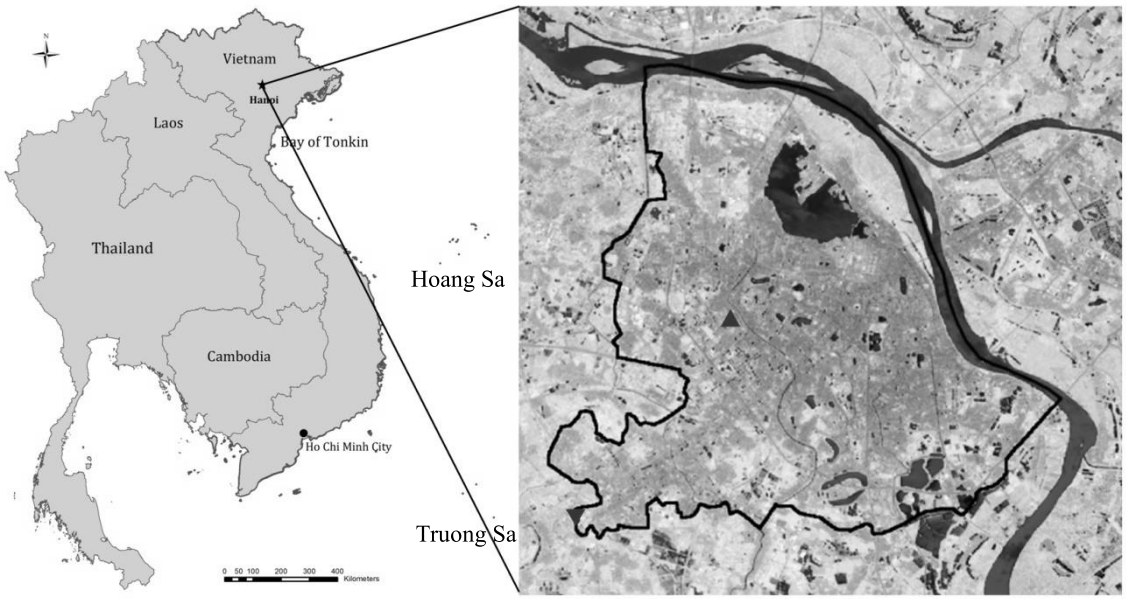


*Figure 1.* Location of the study area, Hanoi inner city, delineated (black polygon) over the false color composite (Shortwave Infrared, Near Infrared, Green) Landsat 8 image taken on 4 June 2017. Locations of the meteorological stations: Lang (black solid triangle) and Ha Dong (black inverted solid triangle) used to access the air temperature data in the research are also presented over the false color composite image

### *2.2. Acquisition and pre-processing of satellite data*

We acquired the Landsat 8 OLI (Operational Land Imager) and TIRS (Thermal Infrared Sensor) images from the same day (June 4, 2017), when Hanoi experienced a heat wave that was more than the hottest level recorded in the past 40 years. On that day, the air temperature in Hanoi reached up to 42°C. The OLI data was converted into Top-Of-Atmosphere (TOA) spectral reflectance applying the rescaling coefficients available in the metadata file.

We also acquired and processed the Landsat 8 OLI and TIRS images taken on another very hot day (June 1, 2016) and a cold day (October 7, 2016) in order to validate the correlation established between heat islands and land-cover composition by comparing them with the images of year 2017. All the Landsat 8 images utilized in the research were cloud free over the study area.

### *2.3. Land-cover mapping and validation*

We adopted the ISODATA-based (Iterative Self-Organized Data analysis) unsupervised classification approach for mapping the three major land-cover types, built-up area, water, and vegetation, which were prevalent in inner Hanoi. We carried out tasseled cap transformation for the Landsat 8 OLI image (June 4, 2017) and calculated three tasseled cap indexes, Greenness, Wetness, and Brightness, following the methodology and transformation coefficients (Table 1) provided by Baig et al. (2014).

These three tasseled cap indexes were used for the ISODATA-based clustering and unsupervised mapping of land-cover types. The newly produced map was validated with the support of ground truth data, which were prepared in the research. We chose randomly 100 geo-location points belonging to the no-changed area between 01 June 2016 and 04 July 2017 of each land-cover class plus

changed-areas of all classes, plus Others class and plus a buffer zone of 3 pixels to validate the classification results. A total of 300 points (for three target classes) were selected. The random points were checked through visual interpretation of Google Earth images and Google Map, acquired in June 2016 and August 2017, respectively. The distribution of the chosen points is displayed in Fig. 2.

*Table 1*. Tasseled cap transformation coefficients for Landsat 8 at-satellite reflectance of five bands: Blue, Green, Red, Near infrared (Nir), Shortwave infrared (Swir 1), and Shortwave infrared (Swir 2)

| Tasseled cap indexes | Landsat 8 bands | | | | | |
|---|---|---|---|---|---|---|
| | Blue (Band 2) | Green (Band 3) | Red (Band 4) | Nir (Band 5) | Swir 1 (Band 6) | Swir 2 (Band 7) |
| Brightness | 0.3029 | 0.2786 | 0.4733 | 0.5599 | 0.508 | 0.1872 |
| Greenness | -0.2941 | -0.243 | -0.5424 | 0.7276 | 0.0713 | -0.1608 |
| Wetness | 0.1511 | 0.1973 | 0.3283 | 0.3407 | -0.7117 | -0.4559 |

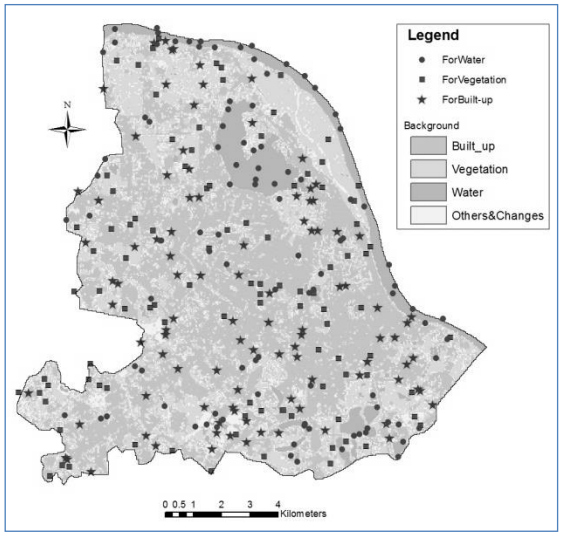


*Figure 2*. Distribution of the ground truth points collected in the research

### *2.4. Mapping of land surface temperature*

Land surface temperature (LST) maps were generated by using the thermal infrared bands 10 and 11, which are available in the Landsat 8 TIRS images (June 4, 2017, June 1, 2016, and October 7, 2016). We applied the Split Window Algorithm (Equation 1) from the literature (Sobrino and Raissouni 2000; Jimenez-Munoz et al., 2014) for the generation of these LST maps.

$$LST = Ti + c1(Ti - Tj) + c2(Ti - Tj)^2 + c_0 + (c3 + c4w)(1 - \mathcal{E}) + (c5 + c6w)\Delta\mathcal{E} \quad (1)$$

In Equation 1, Ti and Tj are the at-sensor brightness temperatures at the thermal infrared bands i and j (in Kelvins) where,

$\mathcal{E}$ is the mean emissivity, $\mathcal{E} = 0.5 (\mathcal{E}i + \mathcal{E}j)$;

$\Delta\mathcal{E}$ is the emissivity difference, $\Delta\mathcal{E} = (\mathcal{E}i - \mathcal{E}j)$;

$w$ is the total atmospheric water vapor content (in g.cm$^{-2}$);

$c0$ to $c6$ are SW coefficients to be determined from simulated data.

Ti and Tj were calculated on the basis of the following formula (Equation 2):

$$T = \frac{K_2}{Ln(\frac{K_1}{L_\lambda}+1)} \quad (2)$$

In Equation 2,

T is at-sensor brightness temperatures;

$L_\lambda$ is TOA spectral radiance in W/(m$^2$ ster μm);

$K_1$ and $K_2$ are the pre-launch calibration constants (from metadata file of Landsat 8 image).

The TOA spectral radiance ($L_\lambda$) (in Equation 2) were calculated from the radiance rescaling factors provided in the metadata file applying the following formula (Equation 3):

$$L_\lambda = M_L Q_{cal} + A_L \quad (3)$$

In Equation 3,

$M_L$ is the band-specific multiplicative rescaling factor;

$A_L$ is the band-specific additive rescaling factor;

$Q_{cal}$ is the quantized and calibrated standard product pixel digital numbers (DN).

The Land Surface Emissivity ($\varepsilon$) was estimated from the Landsat 8 imagery using the NDVI thresholds method (Yu et al., 2014).

The total atmospheric water vapor content coefficient was obtained from NASA's Atmospheric Correction Parameter Calculator (http://atmcorr.gsfc.nasa.gov/).

The coefficients c0–c6 (in Equation 1) were determined from the simulated data provided by Jimenez-Munoz et al. (2014).

The reliability of the Landsat 8 TIRS imagery-based LST maps generated during the research were evaluated taking into account the air temperature data observed by the two meteorological stations in the city.

### *2.5. Preparation of statistical datasets*

A recently produced and validated 30m resolution land-cover map (June 4, 2017) of inner Hanoi was used to prepare the land-cover composition datasets for the research. We applied the moving window method with varying window sizes, from 120 × 120 m (4 × 4 pixels) to 570 × 570 m (19 × 19 pixels), for the preparation of the land-cover composition datasets. We utilized the moving window (distance between the windows is 5 × 5 pixels) through the study area to gather a sufficient number of samples (as large as 7,770) for the statistical analysis. For each window, the percentage coverage of the land-cover types, urban built-up (%U), vegetation (%V), and water (%W), were calculated. We also calculated the mean of the land surface temperature ($\mu$LST) for each window.

### *2.6. Regression analysis and modeling*

The statistical datasets constituting land-cover composition (%U, %V, and %W) and land surface temperatures ($\mu$LST) with varying window sizes (from 120 × 120 m to 570 × 570 m) were used to analyze the relationship between land-cover composition and land surface temperature by performing a regression analysis on the hottest day of 2017. Based on these relationships, a multivariate regression model has finally been established for the prediction of land surface temperature from the land-cover composition. According to the European Green Capital report (EGC 2018), the number of houses located at a distance of more than 300 m from a 0.5 ha adjacent green (or larger) is considered as a basis for the evaluation of a green city. If this number is large, the green score of the city will be reduced. It means that the smallest urban area used for evaluation is around 28 ha (=3.14*300 $m^2$). In addition, the Ministry of Construction of Vietnam issued a Circular No. 10/2008/TT-BXD to guide the assessment and recognition of model new urban centers on 22 April 2008. In the Circular, the first requirement is that the urban area must be 50 ha or more. We assumed that a window size of 510 × 510 m, 17 × 17 pixels of Landsat 8 image, close to 25 ha (half of the minimum requirement of the Circular No. 10) can be considered representative enough as a suitable unit for urban land management and planning. The performance of the newly established model with 510 × 510 m window size was assessed for the prediction of LST with different window sizes on the hottest day of 2017 as well as of 2016. Implications of the established model for urban planning and design were discussed.

The outline of the research methodology is depicted in Fig. 3.

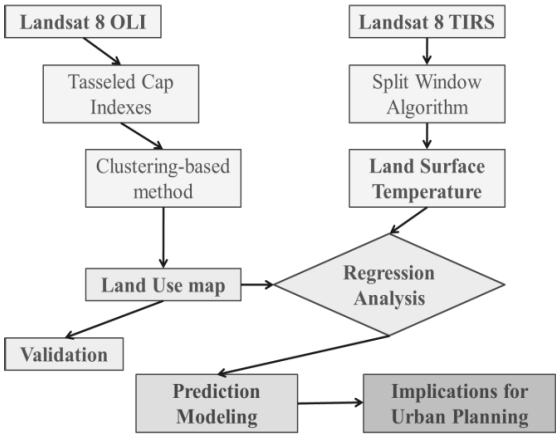


*Figure 3*. Outline of the research methodology

## 3. Results and Discussion

### *3.1. Land cover map and validation results*

The newly produced, 30 m resolution, land-cover map of Hanoi in 2017 is displayed in Fig. 4. The map represents the three major land-cover types, built-up area, vegetation, and water bodies; other types also exist in Hanoi. The accuracy of the newly produced map was validated through the ground truth data prepared in the research. The validation results presented 98% overall accuracy of the map 97%, 98%, and 99% accuracy for the urban built-up area, vegetation, and water respectively.

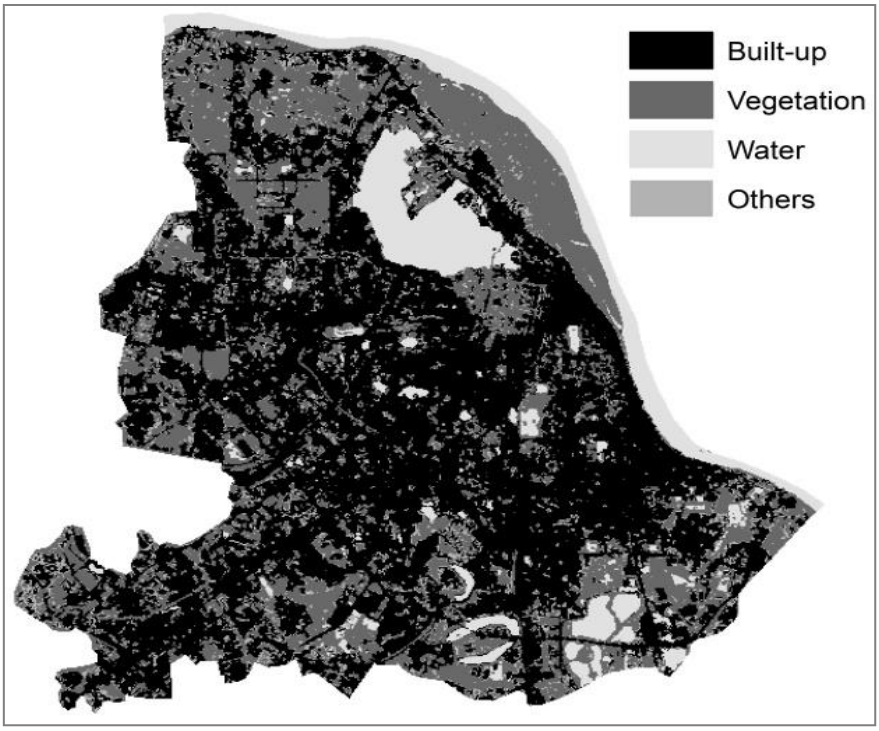


*Figure 4*. Land-cover map of inner Hanoi city of 2017

### *3.2 Land surface temperature maps*

The land surface temperature (LST) maps generated in the research are shown in Fig. 5. According to Jimenez-Munoz et al. (2014), the mean error of the LST is less than 1.5 K. As observed in the maps, significantly high LST (nearly 54.6°C in pixel case) was prevalent at the core of Hanoi city on the hottest day (June 4, 2017).

The LST maps (Fig. 5) demonstrate that the central area of Hanoi exhibited the highest LST compared to the surrounding peri-urban areas. The areas covered by vegetation and water bodies presented lower LST than locations covered by dense urban built-up areas.

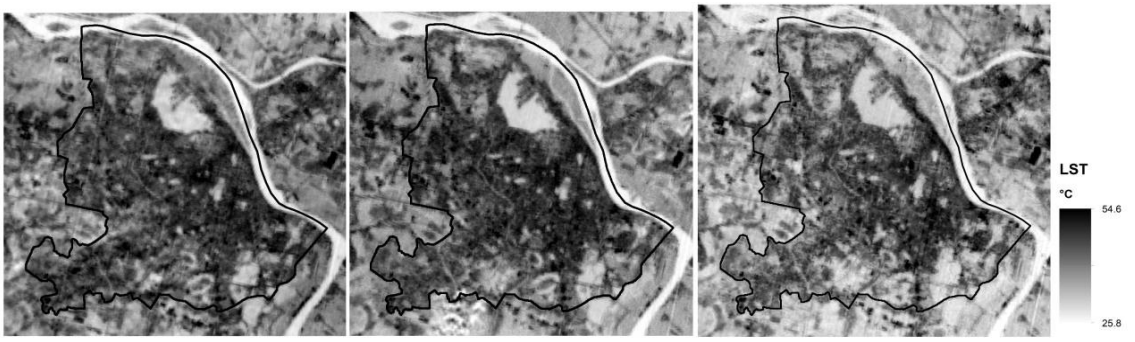


(a) (b) (c)

*Figure 5*. Land surface temperature maps of inner Hanoi city: (a) June 4, 2017; (b) June 1, 2016; (c) October 7, 2016

### *3.3 Comparison of air temperature data*

The air temperature (in °C) data from two meteorological stations in Hanoi observed on June 4, 2017, are collated in Table 1. During the morning (10–11 am) when the Landsat 8 data were captured, the air temperature (38.6–39.6°C) of Ha Dong station situated at a peri-urban region was slightly higher than that of Lang station (37.8–38.7°C) situated at the city center. The LST map generated in the research matched the trend of the air temperature data; the LST from Ha Dong station's pixel case (41.02°C) is slightly lower than that of Lang station (41.19°C) and indicates the robustness of our LST map. From the physical point of view, LST and air temperature are different entities. However, a strong correlation has been described between them by many researchers (Gallo et al., 2011; Schwarz et al., 2012; Mutiibwa et al., 2015; Hadria et al., 2018). Moreover, a similar trend was observed in this study. Therefore, the LST map generated in the research can explain the variability of air temperature and thereby the phenomenon of urban heat islands.

*Table 1*. Comparison of land surface temperature and air temperature data

| Station | Date | Air temperature (°C) in every hour | | | | | | | | | LST (2017-6-4) |
|---|---|---|---|---|---|---|---|---|---|---|---|
| | | 9 | 10 | 11 | 12 | 13 | 14 | 15 | 16 | 17 | |
| Lang | 2017-6-4 | 36.2 | 37.8 | 38.7 | 39.5 | 40.3 | 40.7 | 41.2 | 41.6 | 41.3 | 41.19 °C |
| Ha Dong | 2017-6-4 | 37.3 | 38.6 | 39.6 | 40.2 | 41.0 | 41.5 | 41.4 | 42.5 | 41.8 | 41.02 °C |

### *3.4. Individual land cover coverages versus LST*

Results from the regression analysis showed that there were strong correlations established between the percentage coverage of the individual land-cover types (%U, %V, and %W) and mean land surface temperatures (μLST) for all window sizes considered in the research. However, in our studied area, we detected that smaller window sizes (less than 300×300 m) did not represent a heterogeneous mixture of the land-cover composition. In most cases, one or two components of the land-cover composition (%W, %U, and %V) were absent. Therefore, we present the analysis results pertaining to window sizes larger than 300 × 300 m. On the other hand, the correlation between the percentage coverage of the land cover types (%U, %V, and %W) and mean land surface temperatures (μLST) were much stronger in large window sizes than in small window sizes.

Figure 6 demonstrates the relationships between the percentage coverage of the land-cover types (%U, %V, and %W) and mean land surface temperatures (μLST) in the case of the 510 × 510 m window size. All the

observed relationships were strong; water coverage (%W) showed the highest regression coefficients ($R^2$ = 0.70) followed by urban built-up cover (%U) ($R^2$ = 0.67) and vegetation cover (%V) ($R^2$ = 0.43). It should be noted that water (%W) and vegetation (%V) coverages displayed a negative correlation to µLST, whereas the urban built-up cover (%V) was positively correlated to µLST.

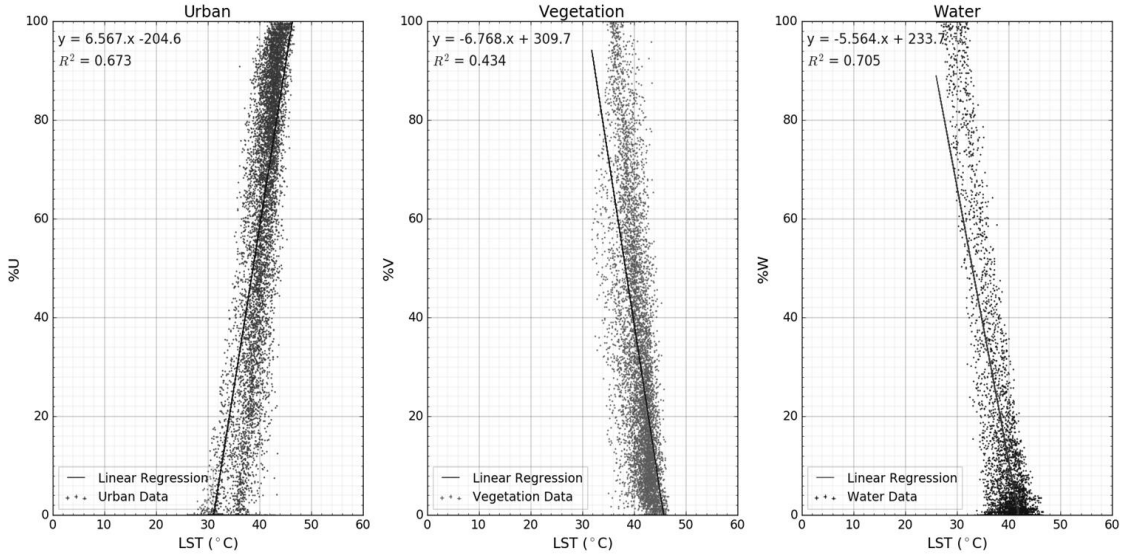


(a) (b) (c)

*Figure 6*. Relationships between percentage coverage of land-cover types (%U, %V, and %W) and mean land surface temperatures (µLST) on the hottest day of 2017 (June 4): (a) µLST and Urban; (b) µLST and Vegetation; (c) µLST and Water

### *3.5. Land-cover composition-driven prediction of LST*

In this research, we established the multivariate regression function between land-cover composition (percentage coverage of urban built-up area (%U), vegetation (%V), and water (%W)) and land surface temperature (LST) on the hottest day of 2017 (June 4). For this purpose, we utilized a 510 × 510 m window size, close to 25 ha, which we assumed to be a suitable unit for urban land management and planning. The resultant regression function is given in Equation 4.

$$LST = 0.032261 \times \%U - 0.040953 \times \%V - 0.137770 \times \%W + 42.01 \quad (4)$$

We analyzed the ability of the established regression function (Equation 4) with a 25 ha land management unit for the prediction of LST with different window sizes. For all window sizes (from 300 × 300 m to 570 × 570 m), the regression function offered stable results (R2 ~ 0.9 in all cases). For example, almost 90% of the variation in LST could be predicted through the established model for the window sizes of 330 × 330 m and 510 × 510 m (Fig. 7). This analysis confirmed that the regression function established using the 510 × 510 m window size can be applied for the prediction of LST with other window sizes as well.

We also tested the ability of the established regression function (Equation 4) for the prediction of LST on the hottest day of 2016 (June 1). Figure 8 presents the successful prediction ($R^2$ > 0.86) of the LST for window sizes 330 × 330 m and 510 × 510 m in this case.

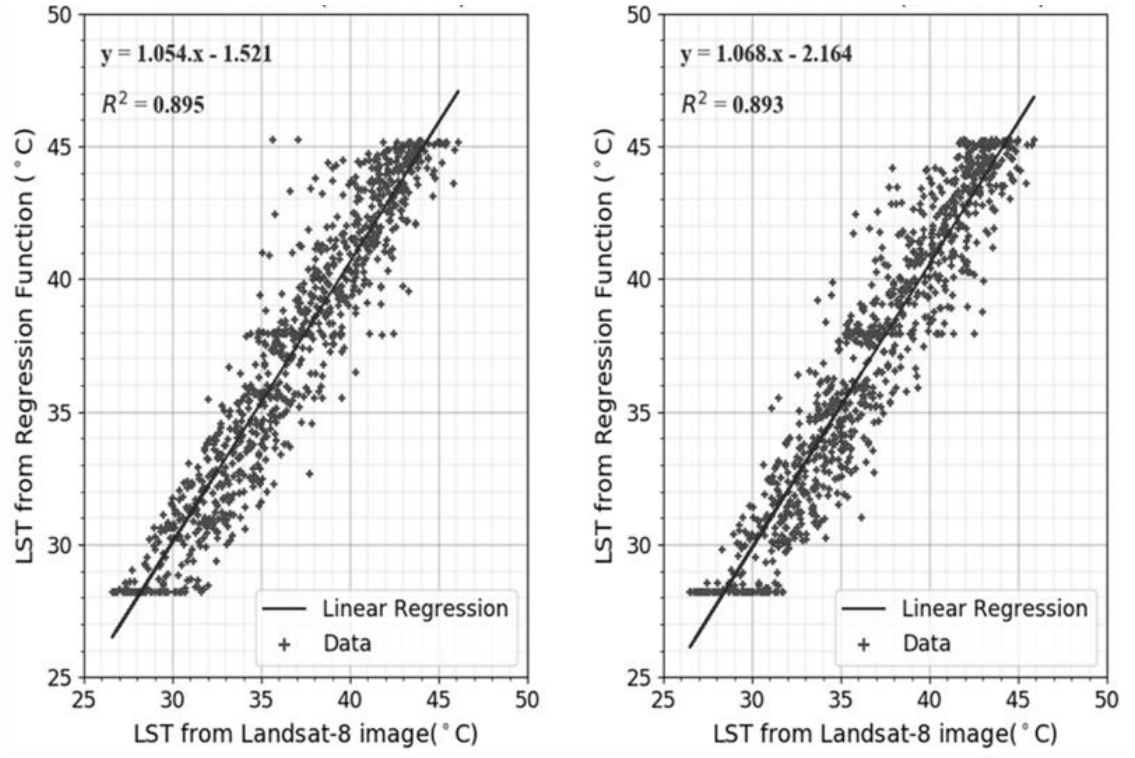


a b

*Figure 7*. Land-cover composition-driven predictions of LST for the hottest day of 2017 (June 4): (a) in the case of 510 × 510 m window size and (b) in the case of 330 × 330 m window size

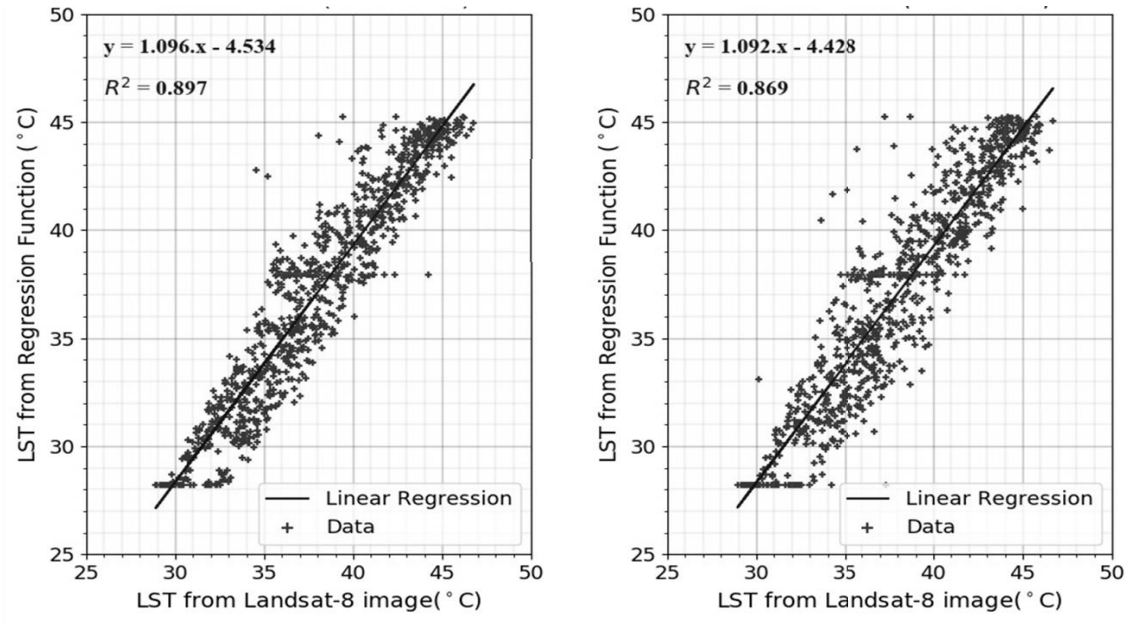


a b

*Figure 8*. Land-cover composition-driven predictions of LST for the hottest day of 2016 (June 1): (a) in the case of 510 × 510 m window size and (b) in the case of 330 × 330 m window size

We further analyzed the applicability of the established regression function for the prediction of LST on a cold day in 2016 (October 7). In case of both window sizes (330 × 330 m and 510 × 510 m), the regression function could successfully predict ($R^2$ > 0.83) the LST (Fig. 9). These analyses confirmed the reliability and applicability of the model established in this research for the prediction of LST in Hanoi with respect to land-cover composition, considering an urban land management unit of 25 ha.

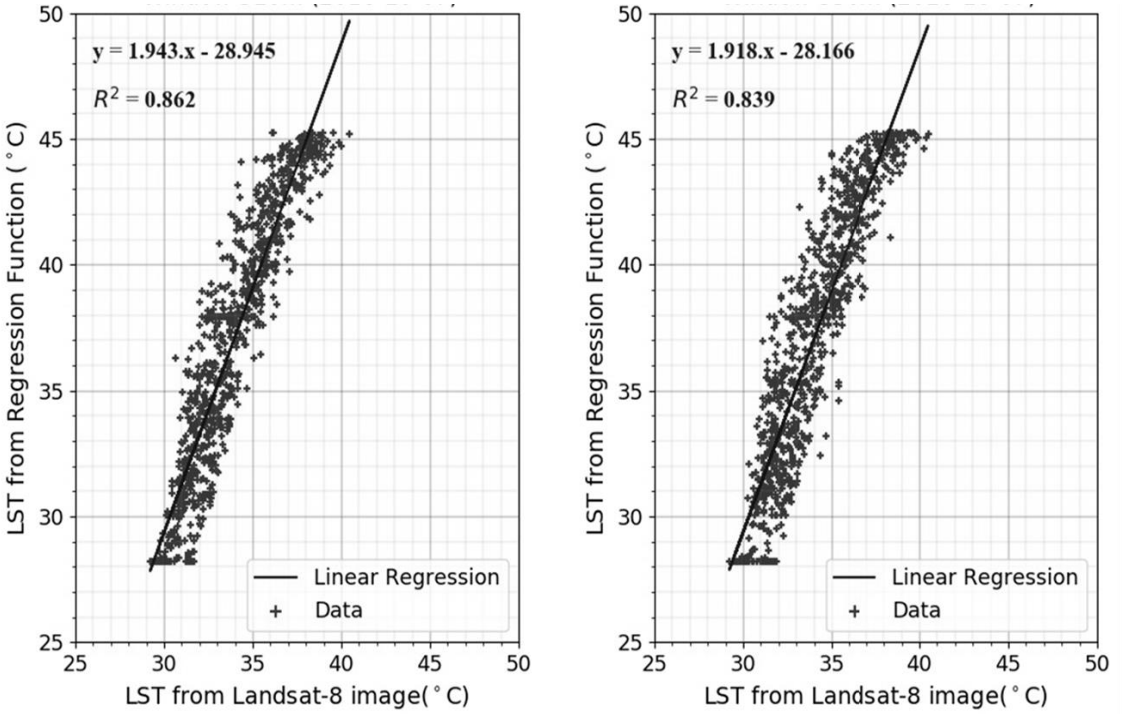


*Figure 9*. Land-cover composition-driven predictions of LST for a cold day of 2016 (October 7): (a) in the case of 510 × 510 m window size and (b) in the case of 330 × 330 m window size

### *3.6. Implications for urban planning and design*

Assuming that the unit of urban land management is around 25 ha (510 m × 510 m), on a very hot day such as June 4, 2017, the LST (in ℃) can be predicted with respect to land-cover composition using the regression model established in this research as shown in Table 2.

The substantial impact of land-cover composition on LST and surface urban heat islands is apparent from Table 2. This analysis shows that LST at each management unit (e.g., 25 ha) can be decreased from 45.23°*C* (100% urban built-up cover) to 37.91°*C* (100% vegetative cover) and then to 28.24°*C* (100% water cover). The urban planner and designer can indeed neither change LST directly to mitigate the effects of surface urban heat islands, nor would it be possible to convert all urban built-up coverage in the cities to water bodies or vegetative areas. However, even a 20% conversion of urban built-up areas into vegetative and water bodies could reduce LST by 2.43°*C*. The results of this research present a wonderful opportunity for urban planners and designers; the LST and associated effects of surface urban heat islands can be

adjusted by managing land-cover composition and percentage coverage of the individual land-cover types (%U, %V, and %W) in each urban land management unit.

*Table 2*. Land-cover composition-driven prediction of land surface temperature

| Land-cover composition | | | LST (in °C) |
|---|---|---|---|
| %U | %W | %V | |
| 100 | 0 | 0 | 45.23 |
| 0 | 0 | 100 | 37.91 |
| 0 | 100 | 0 | 28.24 |
| 80 | 10 | 10 | 42.80 |
| 60 | 20 | 20 | 40.37 |

## 4. Discussions

Reduction in the greenery has been described as a major cause of the rising temperatures in cities by many researchers, and it has been suggested that urban greening activities are the efficient nature-friendly solutions for mitigating urban heat island effects (Rotem-Mindali et al., 2015; Kardinal Jusuf et al., 2007; Zaeemdar and Baycan, 2017; Tang et al., 2017; Lin et al., 2017; Keeratikasikorn et al., 2018; Nastran et al., 2018).

Over the last century, the city of Hanoi has seen a drastic increase in population, high-speed urbanization, and transformation of natural forests into urban built-up areas. All these socioeconomic and biophysical changes have had a critical impact on the urban microclimate. As a result, severe heat waves have become common during the summer months in recent years.

The effects of surface urban heat islands have serious consequences on the lives of urban residents, especially in tropical countries. The research recommends the mitigation of urban heat island effects by increasing green infrastructures, such as roadside plantation, green roofs, city parks, as well as water ponds, which can be installed even in city centers through urban planning initiatives and public awareness. This can promote comfortable and sustainable living in cities.

## 5. Conclusions

In this research, we analyzed the correlation between land-cover composition, percentage coverage of the land cover types (% urban, % vegetation, and % water), and land surface temperature (LST) for different window sizes or urban land management units. Landsat 8 OLI (Operational Land Imager) satellite data was utilized for preparing land-cover composition datasets in inner Hanoi by employing the unsupervised image clustering method. High-resolution (30 m) LST maps were generated for different days of the years 2016 and 2017 using Landsat 8 TIRS (Thermal Infrared Sensor) images.

High correlations were observed between percentage coverage of the land-cover types (%urban, %vegetation, and %water) and LST, coherent with previous studies, considering different window sizes on the hottest day of 2017 (June 4). The vegetation and water coverages demonstrated strong positive correlations to LST, whereas the urban coverage was indirectly proportionate to LST.

Based on the ideas from the results presented above, a multivariate regression model was developed for the correlation between land-cover composition and LST. This land-cover composition–driven model could predict LST efficiently not only in the case of different window sizes but also on different days. The newly developed model in this research provides a wonderful opportunity for urban planners and designers to takes measures for adjusting LST and the associated effects of surface urban heat islands by managing the land cover composition and percentage coverage of the individual land-cover types (%urban, %vegetation, and %water). This model proposes that a substantial decrease in LST can be achieved by increasing the proportion

of vegetation and water for the promotion of comfortable and sustainable living in the city.

## Acknowledgments

This research was funded by Vietnam Academy of Science and Technology (VAST) under project code: UQĐTCB.02/19-20 and KHCBTĐ.02/19-21.

## References

Ackerman B., 1985. Temporal March of the Chicago Heat Island. Journal of Climate and Applied Meteorology, 24, 547–554. Doi: 10.1175/1520-0450 (1985) 024 <0547 TMOTCH >2.0.CO;2.

Baig M.H.A., Zhang L., Shuai T., Tong Q., 2014. Derivation of a tasselled cap transformation based on Landsat 8 at-satellite reflectance. Remote Sensing Letters, 5, 423–431. Doi: 10.1080/2150704X.2014.915434.

Bornstein R.D., 1968. Observations of the Urban Heat Island Effect in New York City. Journal of Applied Meteorology, 7, 575–582. Doi: 10.1175/1520-0450 (1968) 007 < 0575:OOTUHI >2.0.CO;2.

Chen X.-L., Zhao H.-M., Li P.-X., Yin Z.-Y., 2006. Remote sensing image-based analysis of the relationship between urban heat island and land cover/cover changes. Remote Sensing of Environment, 104, 133–146. Doi: 10.1016/j.rse.2005.11.016.

Dihkan M., Karsli F., Guneroglu A., 2015. Guneroglu, N. Evaluation of surface urban heat island (SUHI) effect on coastal zone: The case of Istanbul Megacity. Ocean Coast. Manag, 118, 309–316.

EGC (European Green Capital) Report: Green Urban Spaces with Integration of Sustainable Land cover. Available online: http://ec.europa.eu/environment/europeangreencapital/wp-content/uploads/2016/12/Indicator-3-Green-urban-areas_Nijmegen-2018-revised.pdf (accessed on 11 April 2019).

Estoque R.C., Murayama Y., Myint S.W., 2017. Effects of landscape composition and pattern on land surface temperature: An urban heat island study in the megacities of Southeast Asia. Science of the Total Environment, 577, 349–359. Doi: 10.1016/j.scitotenv.2016.10.195.

Gallo K., Hale R., Tarpley D., Yu Y., 2011. Evaluation of the Relationship between Air and Land Surface Temperature under Clear and Cloudy-Sky Conditions. Journal of Applied Meteorology and Climatology, 50, 767–775. Doi: 10.1175/2010JAMC2460.1.

Grover A., Singh R., 2015. Analysis of Urban Heat Island (UHI) in Relation to Normalized Difference Vegetation Index (NDVI): A Comparative Study of Delhi and Mumbai. Environments, 2, 125–138. Doi: 10.3390/environments2020125.

Hadria R., Benabdelouahab T., Mahyou H., Balaghi R., Bydekerke L., El Hairech T., Ceccato P., 2018. Relationships between the three components of air temperature and remotely sensed land surface temperature of agricultural areas in Morocco. International Journal of Remote Sensing, 39, 356–373. Doi: 10.1080/01431161.2017.1385108.

Hokao K., Phonekeo V., 2012. Assessing the impact of urbanization on urban thermal environment: A case study of Bangkok Metropolitan. International Journal of Applied, 2.

Howard L., 1833. The climate of London deduced from meteorological observations made in the metropolis and at various places around it [electronic resource]; Harvey and Darton.

Huong C.T.T., Hang P.T.L., Hang V.T., Tan P.V., 2010. Variations and trends in hot events in Vietnam from 1961-2007. Journal of Science, Natural Siences and Technology, 26, 370–383.

Jimenez-Munoz J.C., Sobrino J.A., Skokovic D., Mattar C., Cristobal, J., 2014. Land Surface Temperature Retrieval Methods From Landsat-8 Thermal Infrared Sensor Data. IEEE Geoscience and Remote Sensing Letters, 11, 232–242. Doi: 10.1016/j.habitatint.2007.02.006.

Kato S., Yamaguchi Y.. 2005. Analysis of urban heat-island effect using ASTER and ETM+ Data: Separation of anthropogenic heat discharge and natural heat radiation from sensible heat flux. Remote Sensing of Environment, 99, 44–54. Doi: 10.1016/j.rse.2005.04.026.

Keeratikasikorn C., Bonafoni S., 2018. Urban Heat Island Analysis over the Land cover Zoning Plan of Bangkok by Means of Landsat 8 Imagery. Remote

Sensing, 10, 440. Doi: 10.3390/rs10030440.

Kardinal Jusuf S., Wong N.H., Hagen E., Anggoro R., Hong Y., 2007. The influence of land cover on the urban heat island in Singapore. Habitat International, 31.

Kim H.H., 1992. Urban heat island. International Journal of Remote Sensing, 13, 2319–2336. Doi: 10.1080/01431169208904271.

Kotharkar R., Surawar M., 2016. Land cover, Land Cover, and Population Density Impact on the Formation of Canopy Urban Heat Islands through Traverse Survey in the Nagpur Urban Area, India. Journal of Urban Planning and Development, 142, 1. Doi: 10.1061/(ASCE)UP.1943-5444.0000277.

Lin P., Lau S.S.Y., Qin H., Gou Z., 2012. Effects of urban planning indicators on urban heat island: a case study of pocket parks in high-rise high-density environment. Landscape and Smith, R.; Lee, X. Evaluating Efforts to Combat the Chicago Urban Heat Island.

Mai N.T, L. Tang-Huang, 2018. Impacts of Urbanization on Urban Heat Island (UHI) and Meteorological Parameters in Hanoi (1998-2016) from Ground-Based and Satellite Observations. The 39th Asian Conference on Remote Sensing (ACRS), Kula Lumpur, 15-19 October 2018.

Meng Q., Zhang L., Sun Z., Meng F., Wang L., Sun Y., 2018. Characterizing spatial and temporal trends of surface urban heat island effect in an urban main built-up area: A 12-year case study in Beijing, China. Remote Sens. Environ., 204, 826–837.

Miao S., Chen F., LeMone M.A., Tewari M., Li Q., Wang Y., 2009. An Observational and Modeling Study of Characteristics of Urban Heat Island and Boundary Layer Structures in Beijing. Journal of Applied Meteorology and Climatology, 48, 484–501. Doi: 10.1175/2008JAMC1909.1.

Mutiibwa D., Strachan S., Albright T., 2015. Land Surface Temperature and Surface Air Temperature in Complex Terrain. IEEE Journal of Selected Topics in Applied Earth Observations and Remote Sensing, 8, 4762–4774. Doi: 10.1109/JSTARS.2015.2468594.

Nastran M., Kobal M., Eler K., 2018. Urban heat islands in relation to green land cover in European cities. Urban Forestry & Urban Greening. Doi: 10.1016/j.ufug.2018.01.008.

Nguyen D.-Q., Renwick J., McGregor J., 2014. Variations of surface temperature and rainfall in Vietnam from 1971 to 2010: Variations of surface temperature and rainfall in Vietnam. International Journal of Climatology, 34, 249–264. Doi: 10.1002/joc.3684.

Nhung T.D, Nguyen T., Hoan Kieu, Soe W. Myint, 2017. Applying GIS and Remote Sensing to study the relationship between urbanization and urban heat island in Hanoi, Vietnam. Southeast Asian Geography Association Conference at Jakarta, Indonesia.

Oke T.R., Maxwell G.B., 1975. Urban heat island dynamics in Montreal and Vancouver. Atmospheric Environment (1967), 9, 191–200. Doi: 10.1016/0004-6981(75)90067-0.

Rotem-Mindali O., Michael Y., Helman D., Lensky I.M., 2015. The role of local land-cover on the urban heat island effect of Tel Aviv as assessed from satellite remote sensing. Applied Geography, 56, 145–153. Doi:10.1016/j.apgeog.2014.11.023.

Saitoh T.S., Shimada T., Hoshi H, 1996. Modeling and simulation of the Tokyo urban heat island. Atmospheric Environment, 30, 3431–3442. Doi: 10.1016/1352-2310(95)00489-0.

Schwarz N., Schlink U., Franck U., Großmann K., 2012. Relationship of land surface and air temperatures and its implications for quantifying urban heat island indicators. An application for the city of Leipzig (Germany). Ecological Indicators, 18, 693–704. Doi: 10.1016/j.ecolind.2012.01.001.

Singh P., Kikon N., Verma P., 2017. Impact of land cover change and urbanization on urban heat island in Lucknow city, Central India. A remote sensing based estimate. Sustainable Cities and Society, 32, 100–114. Doi: 10.1016/j.scs.2017.02.018.

Sobrino J.A., Raissouni N., 2000. Toward remote sensing methods for land cover dynamic monitoring: Application to Morocco. International Journal of Remote Sensing, 21, 353–366. Doi: 10.1080/014311600210876.

Solecki W.D., Rosenzweig C., Parshall L., Pope G., Clark M., Cox J., 2005. Wiencke, M. Mitigation of the heat island effect in urban New

Jersey. Environmental Hazards, 6, 39–49, Doi: 10.1016/j.hazards.2004.12.002.

Tang J., Di L., Xiao J., Lu D., Zhou Y., 2017. Impacts of land cover and socioeconomic patterns on urban heat Island. International Journal of Remote Sensing, 38, 3445–3465. Doi: 10.1080/01431161.2017.1295485.

Van T.T., H.D. Xuan Bao, N.T. Tuyet Mai. Urban thermal environment and heat island in Ho Chi Minh City, Vietnam from remote sensing data. (www.preprints.org). Doi: 10.20944/preprints201701.0129.v1, 2017.

Van T.T., 2014. Monitoring Urban Heat Island in Vietnam with Remote Sensing. International Workshop on Air Quality in Asia, Hanoi, Vietnam, June 24th-26th.

Van T.T., H.D. Xuan Bao, 2010. Study of the Impact of Urban Development on Surface Temperature Using Remote Sensing in Ho Chi Minh City, Southern Vietnam. Geographical Research. https://doi.org/10.1111/j.1745-5871.2009.00607.x.

Weng Q., Lu D., Schubring J., 2004. Estimation of land surface temperature–vegetation abundance relationship for urban heat island studies. Remote Sensing of Environment, 89, 467–483. Doi: 10.1016/j.rse.2003.11.005.

www1, Number of Very Hot days observed at the Hong Kong Observatory, url: http://www.hko.gov.hk/cis/statistic/vhotday_statistic_e.htm, accessed: 21 April 2018.

www2, India facing another summer of deadly heat, url: https://edition.cnn.com/2017/04/24/asia/india-heat-wave-deaths/index.html, accessed: 21 April 2018.

www3, Vietnam records hottest day so far this year in capital of Hanoi, url: http://english.vov.vn/society/vietnam-records-hottest-day-so-far-this-year-in-capital-of-hanoi-350997.vov, accessed: 24 April 2018. VOV news 2018.

Yu X., Guo X., Wu Z., 2014. Land Surface Temperature Retrieval from Landsat 8 TIRS Comparison between Radiative Transfer Equation-Based Method, Split Window Algorithm and Single Channel Method. Remote Sensing, 6, 9829–9852. Doi: 10.3390/rs6109829.

Yuan F., Bauer M.E., 2007. Comparison of impervious surface area and normalized difference vegetation index as indicators of surface urban heat island effects in Landsat imagery. Remote Sensing of Environment, 106, 375–386. Doi: 10.1016/j.rse.2006.09.003.

Zaeemdar S., Baycan T., 2017. Analysis of the Relationship between Urban Heat Island and Land Cover in Istanbul through Landsat 8 OLI. Journal of Earth Science & Climatic Change, 8. Doi: 10.4172/2157-7617.1000423.

Zhou D., Bonafoni S., Zhang L., Wang R., 2018. Remote sensing of the urban heat island effect in a highly populated urban agglomeration area in East China. Science of The Total Environment, 628–629, 415–429. Doi: 10.1016/j.scitotenv.2018.02.074.